Automated Method for Small-Animal PET Image Registration with Intrinsic Validation

Javier Pascau,[1] Juan Domingo Gispert,[2] Michael Michaelides,[3,4,5] Panayotis K. Thanos,[3,4,6] Nora D. Volkow,[4] Juan José Vaquero,[1] Maria Luisa Soto-Montenegro,[1] Manuel Desco[1]

[1]*Unidad de Medicina y Cirugía Experimental, Hospital General Universitario Gregorio Marañón, C/ Doctor Esquerdo 46, 28007, Madrid, Spain*

[2]*Institut d'Alta Tecnologia, CRC Corporació Sanitària, Parc de Recerca Biomèdica de Barcelona, Passeig Marítim, 25 29, 08003, Barcelona, Spain*

[3]*Behavioral Neuropharmacology & Neuroimaging Lab, Department of Medicine, Brookhaven National Laboratory, Building 490, Upton, NY 11973 5000, USA*

[4]*Laboratory of Neuroimaging, National Institute on Alcohol Abuse and Alcoholism, Department of Health and Human Services, National Institutes of Health, Park Building, 12420 Parklawn Drive, MSC 8115, Bethesda, MD 20892 8115, USA*

[5]*Department of Psychology, Stony Brook University, Stony Brook, NY 11794, USA*

[6]*Departments of Psychology, Neuroscience and Biomedical Engineering, Stony Brook University, Stony Brook, NY 11794, USA*

Abstract

Purpose: We propose and compare different registration approaches to align small-animal PET studies and a procedure to validate the results by means of objective registration consistency measurements.

Procedures: We have applied a registration algorithm based on information theory, using different approaches to mask the reference image. The registration consistency allows for the detection of incorrect registrations. This methodology has been evaluated on a test dataset (FDG-PET rat brain images).

Results: The results show that a multiresolution two-step registration approach based on the use of the whole image at the low resolution step, while masking the brain at the high resolution step, provides the best robustness (87.5% registration success) and highest accuracy (0.67-mm average).

Conclusions: The major advantages of our approach are minimal user interaction and automatic assessment of the registration error, avoiding visual inspection of the results, thus facilitating the accurate, objective, and rapid analysis of large groups of rodent PET images.

Key words: Image registration, Positron emission tomography (PET), Validation, Algorithm, Rats

Introduction

Statistical parametric methods (SPM) are commonly used for comparing positron emission tomography (PET) studies of different patients and groups [1]. This process can also be applied to small-animal studies in order to detect subtle changes between groups avoiding the need to manually segment regions of interest in every study. For this purpose, it is necessary to co-register all the images to a common space. High-dimensional warping techniques are used when registering human studies to PET templates [2, 3]. On the contrary, rigid body transformations, with no warping or scaling, are enough to register brains of rats,

Correspondence to: Javier Pascau; *e-mail:* jpascau@mce.hggm.es

given that their anatomy is quite similar within a certain weight range [4]. The use of previously created templates, a common practice on human studies, is of limited application when working with small animals since the experiments may be performed with different rat or mouse strains, weight range, or PET radiotracers. If the template does not correctly represent the population in terms of anatomy and expected intensity distribution, the alignment process may be less precise, as it has been described in humans [5]. This problem can be prevented by avoiding the use of any template and co-registering the dataset to one representative image selected as a reference [6]. The aligned dataset can then be analyzed using SPM methods.

Different registration algorithms have been proposed in the literature [7, 8], and some of them have been specifically applied to small-animal image alignment [4, 9–11]. Small-animal 2-deoxy-2-[^{18}F]fluoro-D-glucose (FDG)-PET studies do not show the same intensity distribution even for images acquired in similar conditions because the resulting image is influenced by several variables, which are not always completely under control, like blood glucose levels preceding the tracer injection or animal stress during FDG uptake (Fig. 1). In this situation, similarity measures based on information theory seem to be the most suitable cost functions for automatic image alignment [4], and the influence of undesired non-brain structures in the registration process can be minimized by masking the images. The main drawback of the alignment process as a whole is that no measurement of the registration error can be obtained. Provided that not all studies are always successfully registered with the automatic method, every aligned image pair must be visually checked and validated.

Fig. 1. Sagittal sections of two FDG-PET rat brain images (nose is up). Differences in contrast are observed: Both images show glucose metabolic activity in the brain, but image on the *right* displays a higher activity in the neck, while this area is almost cold in the image on the *left*. Slight animal condition differences during FDG uptake may be responsible for these differences.

In this paper, we proposed and compared registration approaches that differed in the use of a brain mask on the reference image and described a procedure to validate the registration results by means of objective consistency measurements [12]. To confirm the ability of registration consistency index to assess registration success and accuracy, we tested this methodology on a study group of FDG-PET rat brain images. The results showed that the proposed methodology permitted an intrinsic validation, avoiding the need to visually check the registration quality of every study.

Materials and Methods

Registration Algorithm

FDG PET images of rat brains usually show similar contrast in brain tissues but large differences in other regions surrounding the brain, as for instance the neck or the tongue. These differences can prevent the use of cost functions like summed of squared (or absolute) differences or correlation functions. For this reason, similarity measures based on information theory seem more adequate for addressing the problem; in this work, we have tested normalized mutual information [13] calculated according to the following formula:

$$NMI = \frac{H(A) + H(B)}{H(A,B)}, \qquad (1)$$

where $H(A)$, $H(B)$ are the entropies of images A and B, and $H(A, B)$ is the joint entropy of both images.

There are several implementation issues that become important when working with these kind of similarity measures in order to achieve a correct registration of the images. Our implementation details are the following:

Multiresolution strategy: The registration process consists of two steps performed at different resolutions, in which the reference image is sub sampled when creating the joint histogram. The sub sampling frequency in the final (high resolution) step must match the actual device resolution, which is approximately 1.7 mm for the PET scanner in our study. The reconstructed images will always have voxel sizes smaller than the actual device resolution, so the final step will not require sampling of all image pixels to match the described criteria. Since the images in our study have matrix sizes of 128×128×63 and voxel size of 0.845 mm×0.845 mm×1.21 mm, the multiresolution scheme that we have used sub samples every [4,4,2] voxels in [*x*,*y*,*z*] coordinates, for the first step (low resolution) and every [2,2,1] in the last step (high resolution).

Histogram interpolation: A joint histogram was used to estimate the joint and marginal entropies. Partial volume interpolation was applied when updating the histogram values because it smoothes the cost function as described in [14]. The correct choice of histogram bins is known to be related to the number of pixels available in the images. Taking into account the matrix sizes for small animal PET studies and the sub sampling factors

used, it is not advisable to use the typical value of 256 bins for the joint histogram because in the worse case ([4,4,2] sub sampling) there would only be one pixel per histogram entry on average, producing local minima on the cost function [15]. On the other hand, a very low number of bins would eliminate the contrast differences of the original images preventing the correct estimation of the cost function. In an attempt to balance both needs, we selected 64 bins for the joint histogram estimation.

Image resampling: Interpolation artifacts are a well known source of problems when deriving information theory measures from the joint histogram. Previous works [16] have showed that if the images to be co registered have pixel grids that can be aligned, periodical local maxima appear in the cost function, making more difficult the optimization process. These artifacts can easily be avoided by resampling one of the images to a different voxel sizes [17]. We applied this resampling procedure to the reference image.

Optimization method: Powell optimization was used as this method is not the fastest but assures good convergence [18].

Reference image masking: As we have explained (Fig. 1), FDG PET animal studies show differences in image intensity distribution for structures outside the brain. This could drive the algorithm toward a solution that may not be optimum in terms of strict brain alignment. Since this intensity distribution can vary depending on the particular study, it seems adequate to mask the brain tissue in the reference image so that pixels outside the mask do not contribute to the cost function value. The mask is generated in a semi automatic fashion by an expert user, by means of an in house developed software that combines region growing techniques with some manually placed boundaries [19].

Masking Approaches Tested

The drawback of masking the reference image is that the algorithm convergence may decrease if there is a large transformation between the studies to be registered. That is because the small amount of pixels inside the mask that are used to evaluate the cost function cause a decrease of the algorithm capture range (the portion of the parameter space in which the algorithm is more likely to converge to the correct optimum [20]). Our proposal is to improve the convergence of the registration algorithm by using the whole images in the first multiresolution step (442) and applying the brain mask to the reference image only in the final step (221). With this two step approach, we expect to obtain a rough alignment in the first step and then a precise registration inside the brain in the final one.

To assess the advantages of the proposed masking procedure (M3), we have compared it to other two approaches (M1 and M2):

M1: No brain mask used for registration

M2: Brain mask applied to the reference image on every step (442 and 221)

M3: No mask used for the first step (442); brain mask used in the final step (221)

The scheme of the whole registration process is summarized in Fig. 2.

Reference Images and Registration Consistency

The selection of one image from the dataset to be the common reference for the registration is the standard way to co register specimens and perform voxel wise comparisons with SPM meth ods, when a template of the population is not available. The selection of this image is not trivial as not all images show the same contrast in regions outside the brain. Because of these contrast differences, the registration success of the whole image dataset may depend on the image selected as the reference. Typically, the registration results have to be visually inspected to detect failures, which can still be registered again with some manual interaction. To automate this validation process, we measure the registration consistency, following the idea initially proposed by Woods et al. [12]. This method was also used by Holden et al. [21] to compare similarity measures in serial MRI/MRI registration. It uses three images and their three pairwise registrations and compares one of the transformations with the composition of the other two. In the case of any imperfect registration, the direct transformation will not be equivalent to the composed one, and this difference will serve as an estimate of the registration error.

The registration of the whole dataset to a single reference does not provide enough redundancy to calculate registration con sistency, so we selected two reference images and made use of a known transformation between them to assess the quality of the registration for every image in the dataset. An expert user selected two images from the dataset to serve as the references, avoiding images with poor contrast, animal movement, or low quality. These references, r_1 and r_2, were manually registered using six pairs of anatomical landmarks [22], and the average fiducial registration error (FRE), as defined in [23], was calculated. We call this reference transformation $T_{r_1 r_2}$ and the associated matrix $M_{r_1 r_2}$. Since this transformation is known to be correct, it will allow assigning the error calculated from the registration consistency for every image in the dataset to the automatic registrations.

The same user segmented the brain in both images, thus creating a binary mask used for the registration approaches M2 and M3, applying region growing techniques implemented in an in house developed software [19] as described in "Registration Algorithm". Note that only the two reference images need to be segmented; all the other images in the dataset do not need to be processed.

Every image I_j in the dataset was registered to every reference image, obtaining transformations $T_{I_j r_1}$ and $T_{I_j r_2}$ and the associated homogeneous matrices ($M_{I_j r_1}$ and $M_{I_j r_1}$). This process was repeated for every registration approach M1, M2, and M3. In the absence of registration error, being $\times$ the composition of transformations, $T_{I_j r_1} \times T_{r_1 r_2} \times T_{r_2 I_j}$ should correspond to the identity transforma tion. Thus, the difference between $M_{I_j r_1} \cdot M_{r_1 r_2} \cdot M_{r_2 I_j}$ and the identity matrix I estimates the registration error:

$$\Delta M_j = M_{I_j r1} \cdot M_{r_1 r_2} \cdot M_{r_2 I_j} - I. \quad (2)$$

In an attempt to represent this error with a single number, we selected a bounding box containing our volume of interest (the brain) and calculated the average error in the eight vertices of this box ($p(i)$ $[x_i,y_i,z_i]$ i 1…N, N 8):

$$RCI_j = 1/N \sum_{i=1..N} \left\| \Delta M_j \cdot p(i) \right\|. \quad (3)$$

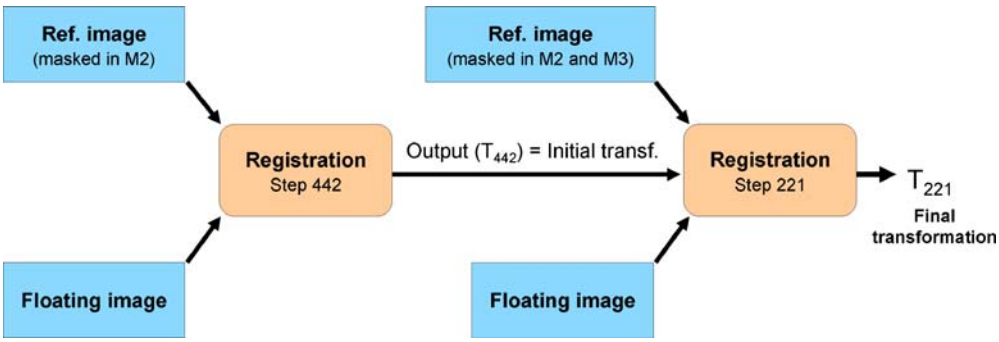

Fig. 2. Registration process with the two multiresolution steps (442 and 221). Reference image is either masked or not at every step depending on the approach proposed (M1, M2, or M3).

This registration consistency index (RCI_j) measures the registration consistency for image I_j and reference images r_1 and r_2. To classify the registration of image I_j with both references as either successful or not, the actual resolution of the system (scanner plus reconstruction algorithm) is used as a threshold, assuming that the registration accuracy should be smaller than that value. Consequently, if RCI_j is lower than the actual system resolution, the registration is classified as *successful*, and when it is larger, the registration result is labeled as *failure*.

Test Dataset

Twenty male adult Zucker rats (7 months old) were used to evaluate the methodology described in the preceding sections. This dataset was part of a study on obesity and food restriction [24]. Each animal was scanned twice at two different experimental conditions. All animals were placed in a head holder (David Kopf Instruments; CA, USA) in a prone position on the bed of the scanner, but stereotaxic measurements were not taken into account. Scanning time was 80 min, with a 40 min FDG uptake (~0.8 mCi). The small animal scanner was a Concorde microPET R4, and all images were reconstructed using the OSEM3D MAP algorithm [25] provided by the manufacturer that claims for an approximate resolution of 1.7 mm [26]. Reconstructed images had a matrix size of 128×128×63 and a voxel size of 0.845 mm×0.845 mm×1.21 mm.

Two reference images (r_1 and r_2) were selected; the brain was segmented on both reference images with the semi automatic procedure previously described and were manually co registered using anatomical landmarks. All images from the dataset were then automatically registered to both references, following the procedure described in previous sections. These automatic registrations were performed three times applying the M1, M2, and M3 masking schemes described in "Registration Algorithm", and the RCI_j value was computed for every image and every scheme. Registration results with RCI_j lower than 1.7 mm (PET scanner actual resolution) were classified as successful, and failure otherwise.

The automatic validation process proposed depends on the manual co registration of the reference images r_1 and r_2. In order to demonstrate the repeatability of this step, it was repeated by three different users independently, and average fiducial registration error was calculated for every co registration.

Visual Validation

To confirm the ability of the registration consistency index to assess registration success and accuracy, every registered image pair (image I_j registered with every reference and for every registration approach M1, M2, and M3) was visually checked by an expert who, depending on the registration quality in the brain tissue (which is the structure of interest), classified the registration as either successful or failure. These registration quality results were then combined, so for every image I_j, both registration results (with both reference images r_1 and r_2) had to be correct to classify the experiment as successful.

Results

Results from the different users who preformed the manual registration (transformation $T_{r_1 r_2}$) of both reference images are summarized in Table 1. Every user manually registered images r_1 and r_2 once. The users achieved similar registration parameters and FRE. This latter parameter provides an estimate of the manual registration accuracy. All users obtained an average FRE around 0.5 mm. Inter-user differences were below 0.5 mm in translations and 2° in rotations. To quantify these differences with a single value, we used the registration consistency index, as defined in Eq. 3, but this time applied to inter-user comparisons, and we obtained values of 0.7602 mm for the User1–User2 comparison, 0.7003 mm for the User1–User3, and 0.6906 mm for the User2–User3. These figures are lower than half the actual system resolution (~1.7 mm) and indicate that inter-user variability for this manual step can be neglected. Parameters obtained by User1 were selected as reference transformation $T_{r_1 r_2}$. The average time needed for manual registration was 5 min.

Table 2 summarizes the registration results obtained with the image dataset for each of the automatic registration approaches (M1, M2, and M3). The number of successful and failed experiments, as classified by the expert (first column) and according to registration consistency (second column), are shown. The third column displays the average of the consistency error values for every row, as a measure of accuracy. Lower values correspond to better accuracy.

Figure 3 displays five cases after a successful registration with reference r_1 using M3 approach, showing how the brain tissue is correctly aligned in all the cases despite the different

intensity distribution of structures outside the brain in every image.

The registration average time per case (registering a single image pair), including both multiresolution steps, was 8, 9, and 8 s, respectively, for methods M1, M2, and M3. These figures demonstrate the high speed of the process. The whole dataset (40 images) is registered to both references in a maximum of 12 min. The total time of registration and intrinsic validation includes image selection (5 min), brain segmentation (about 10 min), and manual registration (5 min) of both reference images. All the steps together take less than 35 min in our test dataset with 40 scans.

Discussion

Results are discussed for every registration approach.

- M1: The use of the whole image without any masking during the registration process produces a low success rate, the worst accuracy for the good registrations (1.06 mm), and a low agreement between visual and automatic methods for calculating registration quality. If the whole image is used to guide the registration process, structures outside the brain may become aligned instead of the brain itself, thus decreasing the registration accuracy in the brain tissue. When these wrong alignments are similar for both reference images, the registration consistency is good, but the visual validation shows an incorrect alignment in the brain tissue. For this reason, successful registration figures are different for both (visual and consistency based) validations. Because of this discrepancy, the accuracy figures for failed registrations (2.68 mm) may not indicate low error, but they can be related to both references producing similar incorrect alignments.
- M2: The approach that masks the reference image at both steps of the registration process has the lowest success rate. This result is consistent with the problem described in the "Materials and Methods" section: The use of a brain mask makes the registration algorithm less stable, and consequently in some cases, it converges to an incorrect transformation. In contrast, those results classified as good show high accuracy because the algorithm ignores any structures outside the brain. Visual and automatic quality checking are in good agreement with this approach; this indicates that when the algorithm works, it converges to the optimum solution.
- M3: This approach combines the advantages of M1 and M2. The use of the whole image at the low resolution step provides robustness, while masking the brain at the high resolution step assures accuracy. The results show the highest success rate (87.5% successful registrations) with similar accuracy than M2. The agreement between both procedures for checking the successful registrations is also good.

The results show that the M1 registration approach converges to incorrect results in most cases. Structures outside the brain can be aligned in a similar incorrect way for both reference images because the brain is not being masked. For this reason, the value of RCI calculated in this approach is not correctly indicating the registration quality because in some cases, a low RCI corresponds to incorrect registrations. M2 is accurate inside the brain tissue but has a low success rate. Finally, M3 combines a rough alignment from the low resolution step with a precise registration in the brain tissue during the last step. Despite the different average consistency of approaches M2 and M3, we cannot conclude that M2 is a more accurate approach than M3 because of the low success rate when using M2.

Although M3 appeared as the best approach for registering FDG-PET rat brain images, even in this case, there were still five registration failures automatically and correctly identified by RCI. These images were manually pre-aligned and registered again, obtaining a good registration (according to visual checking) in all the five cases.

Other authors have registered PET images of the rat brain from different specimens but, to our knowledge, the proposed validation has never been applied to these kind of studies: In [4], the authors validated the results using visual assessment only, and in [27], they estimated the accuracy by applying known misalignments to registered scans and measuring the error for the recovered transformation. This latter method was in fact computing the robustness of the registration algorithm to the applied misalignments, but not the accuracy itself, because it first registers the datasets with the algorithm they propose and then tries to recover this solution after a certain misalignment. This evaluation assumes that the first registration is correct but does not measure its accuracy. The validation procedure proposed in the present study has showed that, when using the M3 approach, the accuracy measured using registration consistency is a good estimate of registration quality. This

Table 1. Manual registration parameters obtained by three different users when aligning reference images

	T_x	T_y	T_z	R_x	R_y	R_z	FRE
User1	−1.479	−0.110	−4.127	0.008	1.583	0.009	0.420
User2	−1.119	−0.561	−4.130	−0.187	−0.208	−1.150	0.498
User3	−1.225	−0.370	−4.439	−1.808	1.127	−0.292	0.411

Translations (Tx, Ty, Tz) in mm and rotations (Rx, Ry, Rz) in degrees. FRE: average fiducial registration error

Table 2. Registration results for the whole image dataset for each approach (M1, M2, and M3 as described in the text)

	Visual check	Consistency	Accuracy
M1: no mask used			
Failure	27	14	2.68
Success	13	26	1.06
Total	40	40	
M2: mask always used			
Failure	29	29	18.07
Success	11	11	0.47
Total	40	40	
M3: mask used in 221 step			
Failure	5	5	18.63
Success	35	35	0.67
Total	40	40	

Number of experiments classified as success or failure according to visual inspection (first column) and using registration consistency (second column) are showed. The third column shows the average accuracy of every group of experiments (success or failure), estimated by registration consistency index.

validation should be used when aligning small animal image datasets since it only requires the user to select two reference images and to segment and manually co-register them. As a result, the procedure provides the registered dataset as well as an estimate of the registration quality for every image. Our results are limited to FDG-PET studies, widely used in small-animal imaging. Further validation would be necessary to apply the proposed methodology to other radiotracers.

Conclusion

This paper compares three different approaches for co-registering small-animal FDG-PET scans, making use of registration consistency for automatically validating the results. The major advantages of our approach over previous ones are (1) minimal user interaction (only the registration checking for the reference images and their brain mask segmentation) and (2) automatic assessment of the registration error for each study. We have shown that the best results, in terms of success rate and registration accuracy, were obtained by the approach that co-registered the whole images in low resolution in a first step and then masked the brain of the reference image during a second high resolution step. Our methodology makes it unnecessary to visually

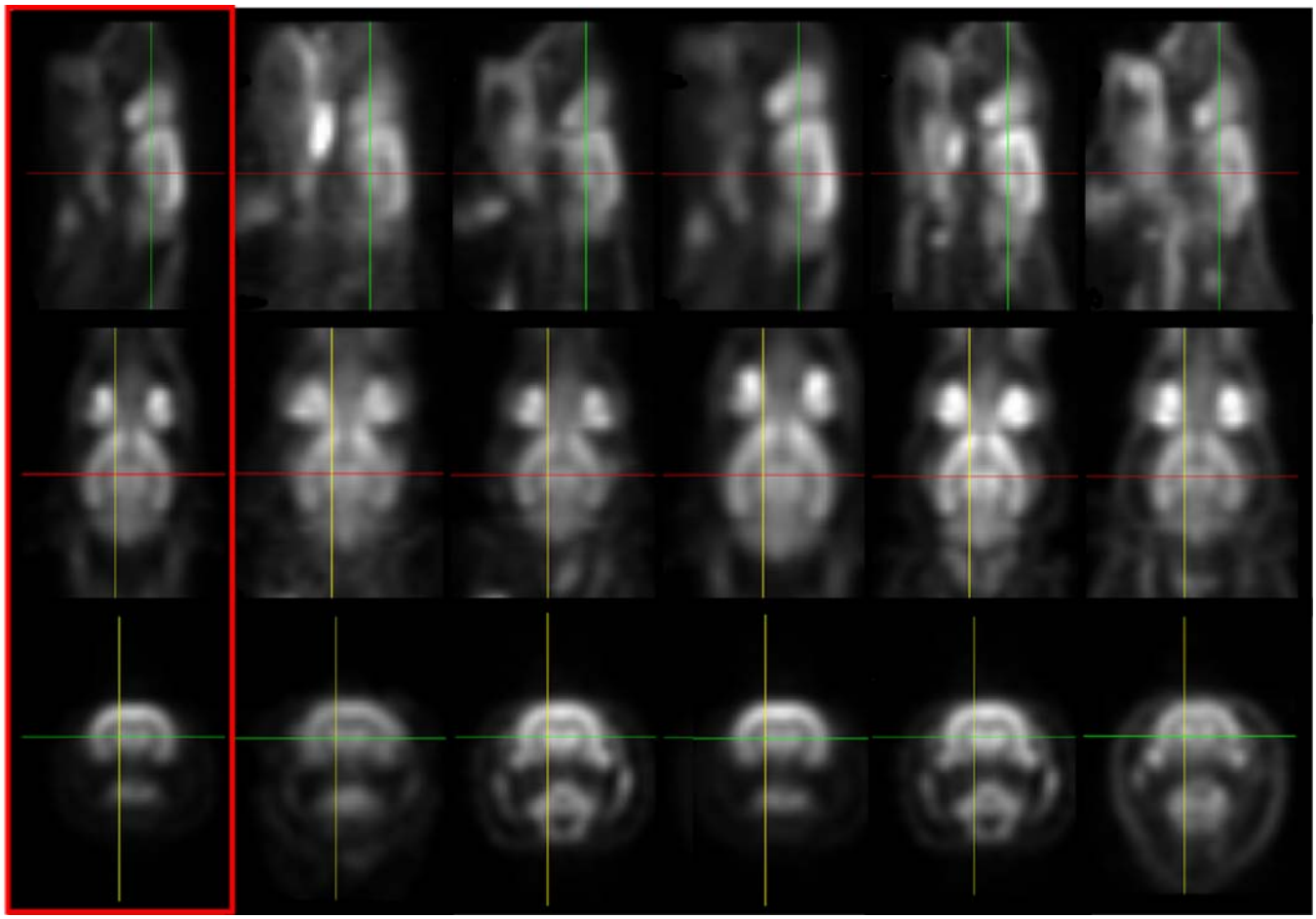

Fig. 3. Sagittal, coronal, and trans-axial views of the reference image r_1 (*first column*) and five example cases of registered images using M3 approach. *Axes* represent the same position for all the registered images. Notice the good alignment in the brain tissue despite the different intensity distribution outside this structure.

inspect and check every registration result and provides an objective assessment of accuracy. This method will thus facilitate the accurate, objective, and rapid analysis of large groups of rodent PET images.

Acknowledgements. This work was supported by projects CIBER CB06/01/0079 (Ministerio de Sanidad y Consumo) and CDTEAM (CENIT program, Ministerio de Industria). Further support came from NIAAA Intramural Research Program (AA 11034 and AA07574, AA07611) and the US Department of Energy (DE-AC02-98CH10886).

References

1. Friston KJ, Holmes AP, Worsley KJ et al (1995) Statistical parametric maps in functional imaging: a general linear approach. Hum Brain Mapp 2:189 210
2. Thompson PM, Woods RP, Mega MS et al (2000) Mathematical/computational challenges in creating deformable and probabilistic atlases of the human brain. Hum Brain Mapp 9(2):81 92
3. Friston KJ, Ashburner J, Frith C et al (1995) Spatial registration and normalization of images. Hum Brain Mapp 2:165 189
4. Rubins DJ, Melega WP, Lacan G et al (2003) Development and evaluation of an automated atlas-based image analysis method for microPET studies of the rat brain. Neuroimage 20(4):2100 2118
5. Gispert JD, Pascau J, Reig S et al (2003) Influence of the normalization template on the outcome of statistical parametric mapping of PET scans. Neuroimage 19(3):601 612
6. Toga AW, Thompson PM (2001) The role of image registration in brain mapping. Image Vis Comput 19(1 2):3 24
7. Pluim JP, Maintz JB, Viergever MA (2003) Mutual-information-based registration of medical images: a survey. IEEE Trans Med Imag 22 (8):986 1004
8. Maintz JB, Viergever MA (1998) A survey of medical image registration. Med Image Anal 2(1):1 36
9. Vaquero JJ, Desco M, Pascau J et al (2001) PET, CT, and MR image registration of the rat brain and skull. IEEE Trans Nucl Sci 48(4):1440 1445
10. Rowland DJ, Garbow JR, Laforest R et al (2005) Registration of F-18 FDG microPET and small-animal MRI. Nucl Med Biol 32(6):567 572
11. Fei BW, Wang HS, Muzic RF et al (2006) Deformable and rigid registration of MRI and microPET images for photodynamic therapy of cancer in mice. Med Phys 33(3):753 760
12. Woods RP, Grafton ST, Holmes CJ et al (1998) Automated image registration: I. General methods and intrasubject, intramodality validation. J Comput Assist Tomogr 22(1):139 152
13. Studholme C, Hill DLG, Hawkes DJ (1999) An overlap invariant entropy measure of 3D medical image alignment. Pattern Recogn 32(1):71 86
14. Maes F, Collignon A, Vandermeulen D et al (1997) Multimodality image registration by maximization of mutual information. IEEE Trans Med Imag 16(2):187 198
15. Thurfjell L, Lau YH, Andersson JL et al (2000) Improved efficiency for MRI-SPET registration based on mutual information. Eur J Nucl Med 27(7):847 856
16. Pluim JP, Maintz JB, Viergever MA (2000) Interpolation artefacts in mutual information based image registration. Comput Vis Image Underst 77(2):211 232
17. Tsao J (2003) Interpolation artifacts in multimodality image registration based on maximization of mutual information. IEEE Trans Med Imag 22(7):854 864
18. Maes F, Vandermeulen D, Suetens P (1999) Comparative evaluation of multiresolution optimization strategies for multimodality image registration by maximization of mutual information. Med Image Anal 3 (4):373 386
19. Pascau J, Vaquero J, Abella M et al (2006) Multimodality workstation for small animal image visualization and analysis. Mol Imaging Biol 8(2):97 98
20. Hill DL, Batchelor PG, Holden M et al (2001) Medical image registration. Phys Med Biol 46(3):R1 R45
21. Holden M, Hill DL, Denton ER et al (2000) Voxel similarity measures for 3-D serial MR brain image registration. IEEE Trans Med Imag 19(2):94 102
22. Arun KS, Huang TS, Blostein SD (1987) Least-squares fitting of two 3-D point sets. IEEE Trans Pattern Anal Mach Intell 9(5):698 700
23. Fitzpatrick JM, West JB, Maurer CR Jr (1998) Predicting error in rigid-body point-based registration. IEEE Trans Med Imag 17(5):694 702
24. Thanos PK, Michaelides M, Gispert JD et al (2008) Differences in response to food stimuli in a rat model of obesity: in-vivo assessment of brain glucose metabolism. Int J Obes (May 13, 2008)
25. Qi J, Leahy RM, Cherry SR et al (1998) High-resolution 3D Bayesian image reconstruction using the microPET small-animal scanner. Phys Med Biol 43(4):1001 1013
26. Ruangma A, Laforest R, Bai B et al (2004) Characterization of USC-MAP image reconstruction on MicroPET-R4. IEEE Nucl Sci Symp Conf Rec 6:3449 3453
27. Casteels C, Vermaelen P, Nuyts J et al (2006) Construction and evaluation of multitracer small-animal PET probabilistic atlases for voxel-based functional mapping of the rat brain. J Nucl Med 47(11):1858 1866